

Bixler 3 Flight Test Analysis

Apoorva Sharma, Justin Schneider, Miao Zhang, Victoria M Dax, Zhe Zhang and Zhengyu Huang
AA241X

Department of Aeronautics and Astronautics
Stanford University, Stanford, CA 94305

2017-4-25

I RC Flight of Bixler 3

The process of assembling the Bixler 3 was relatively simple. The vertical tail and horizontal stabilizer were epoxied together, and then epoxied to the rear of the plane. The two wing halves were joined with an aluminum tube spar and pinned into the fuselage. Also, the landing gear was removed as it was unnecessary. On the electronics side, the transmitter was bound to the Pixhawk mini and various sensors were connected to the Pixhawk such as telemetry, GPS/Compass, the arming signal, the control surface servos, and power. With everything connected, the Pixhawk was then calibrated through QGroundControl. Through this process, it was discovered that the throttle and rudder servo connections were swapped from what was in the documentation. With the radio, accelerometer, gyroscope, and magnetometer all calibrated, the Bixler 3 was ready to fly and record data.

Our pre-flight checklist began with checking the battery voltage and making sure the propeller was firmly secure. The Bixler 3 was then powered on and the direction of the ailerons, elevator, and rudder were double-checked. Then the throttle was armed and tested to determine if there was enough thrust. Finally we would check the QGroundControl reported GPS heading of the plane and compare it to the true plane orientation. If it matched reasonably, we were ready to fly.

II Flight Data for Bixler 3

This section will show the flight data we collected on the morning of the 25th of April. The maximum altitude Bixler3 reached is about 100 meters, the flight trajectory is shown below

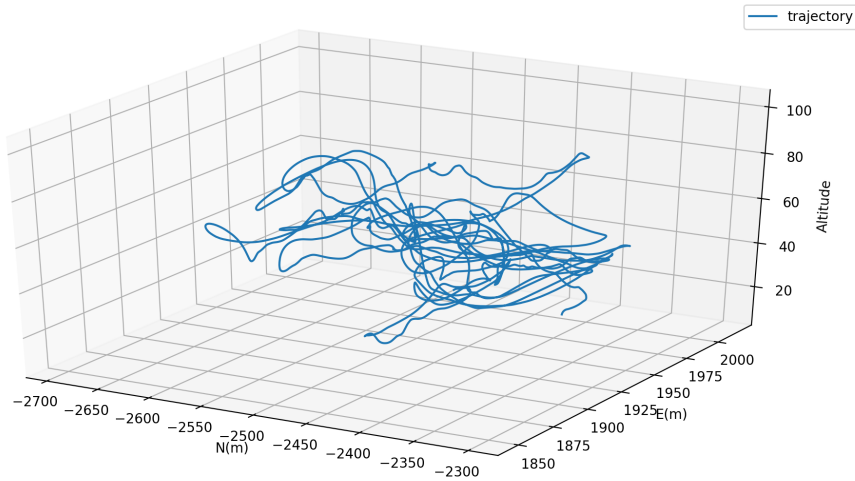


Figure 1: 3D trajectory

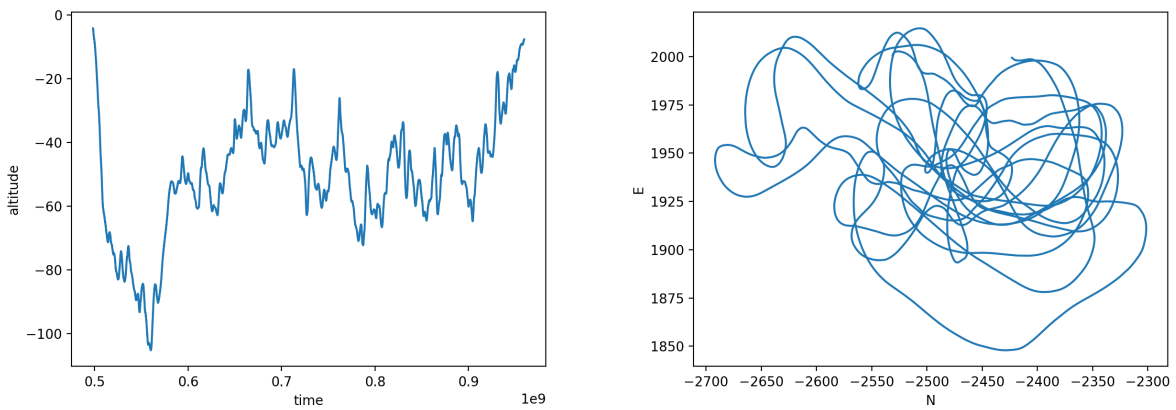


Figure 2: Altitude in downward direction and path in latitude and longitude

The roll pitch yaw angles and their corresponding control inputs are

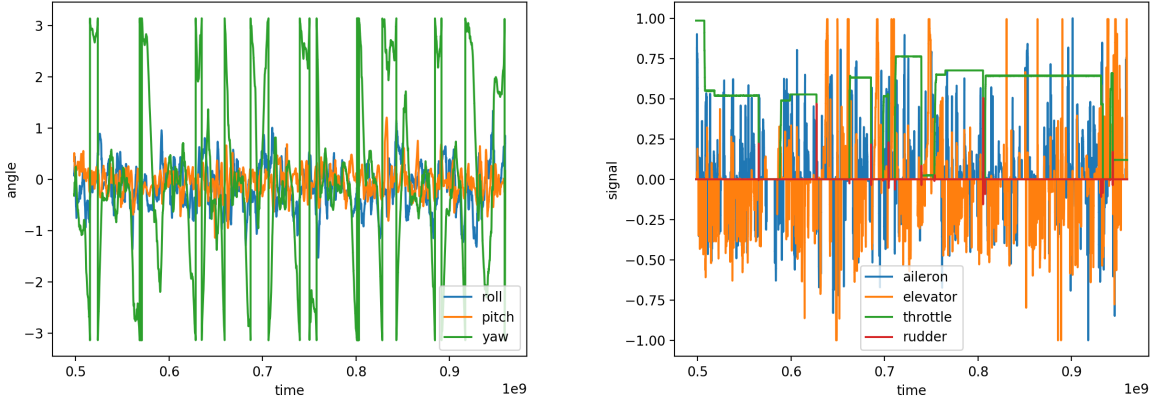


Figure 3: Roll pitch yaw angles and control inputs

The flight velocity in body coordinate and the battery power conditions are

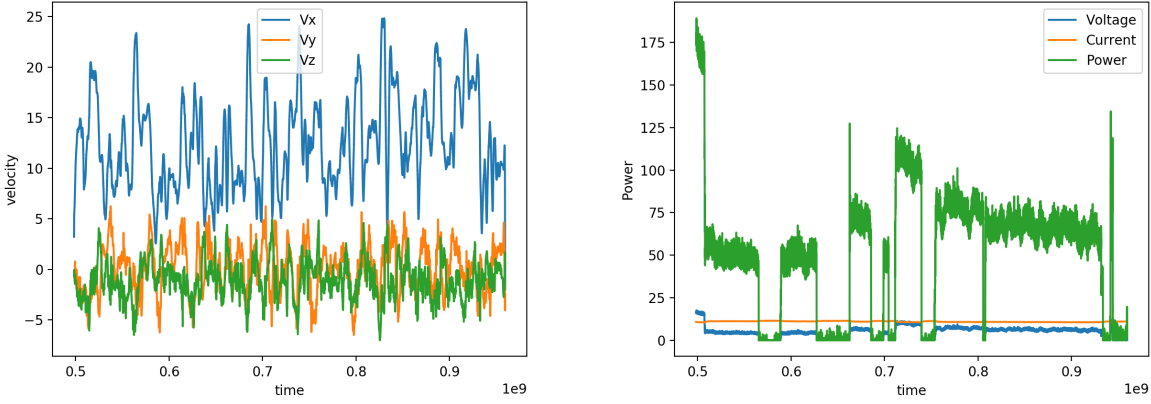


Figure 4: Velocity and Battery condition

To do data analysis, we need to first figure out the portions that were level flight part, and those that were glide flights. To do this, we filtered our data and kept only the parts with throttle off and roll angle less than 3 degrees. We have several sub-trajectories, the altitude and path are shown below:

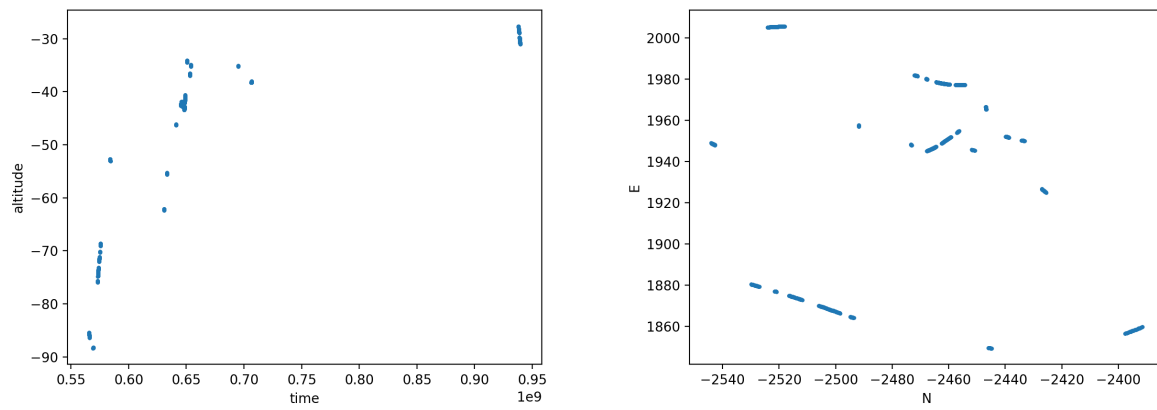


Figure 5: Altitude in downward direction and path in latitude and longitude for no-throttle roll angle less than 3 degrees flight

The roll pitch yaw angles and control inputs of these sub-trajectories are shown below:

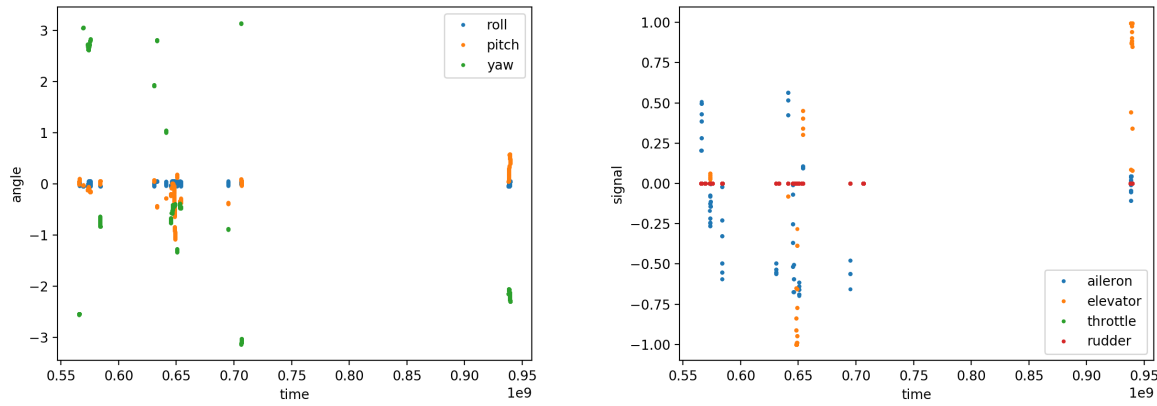


Figure 6: Roll pitch yaw angles and control inputs for no-throttle roll angle less than 3 degrees flight

The velocity and battery conditions for these sub-trajectories are shown below:

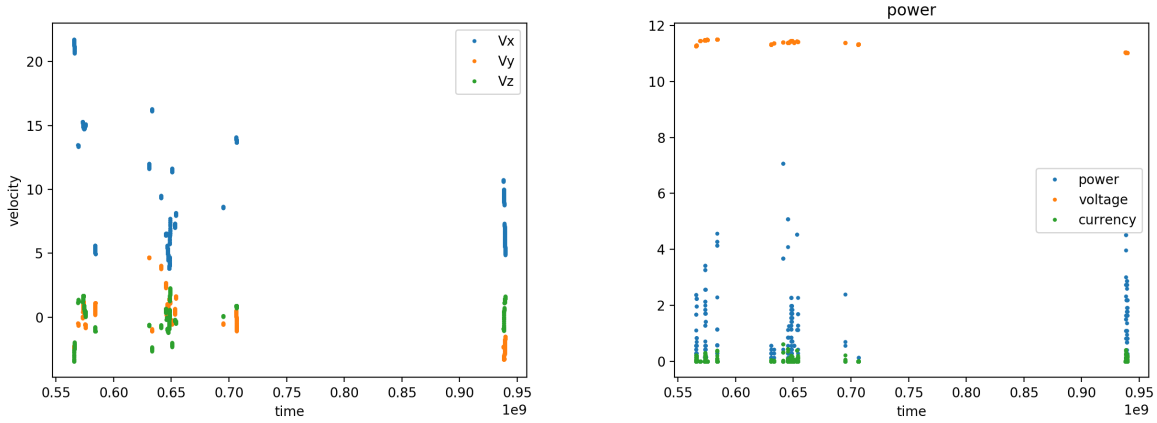


Figure 7: Velocity and Battery condition for no-throttle roll angle less than 3 degrees flight

We tried to let the Bixler glide without any control from 574sec to 582sec; the altitude drops from about 75 meter altitude to 52 meter. The flight trajectory is slightly curved, from (-2508,1870) to (-2555,1950) because of the wind. The glide angle is about 15 degrees.

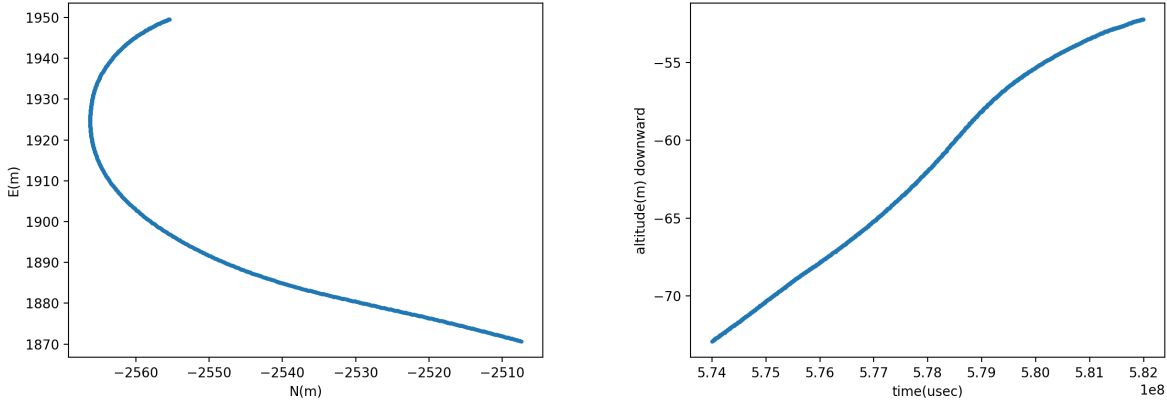


Figure 8: Glide flight trajectory and negative altitude in meters

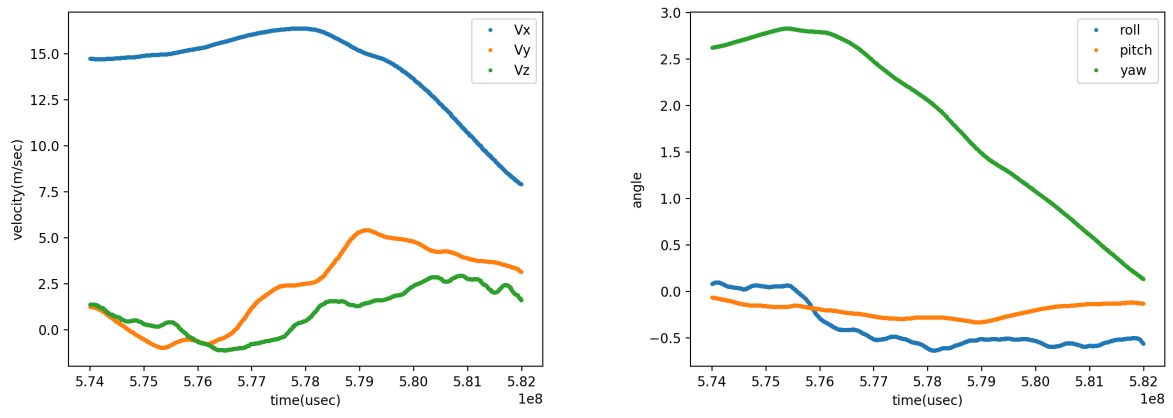


Figure 9: Glide flight velocity and angles

III Theory vs. Experimental Data

III.1 Theoretical Results

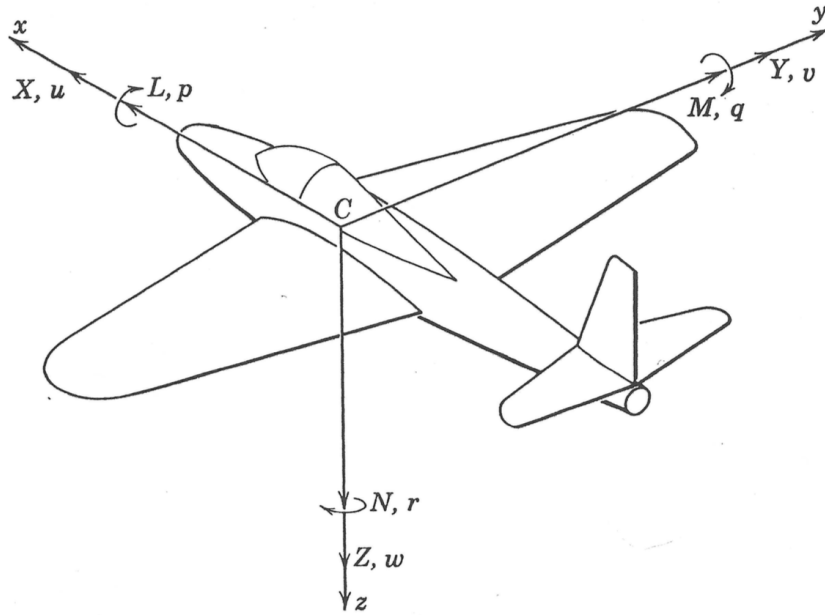
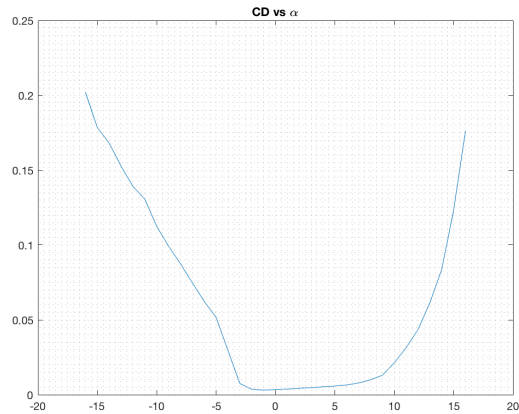
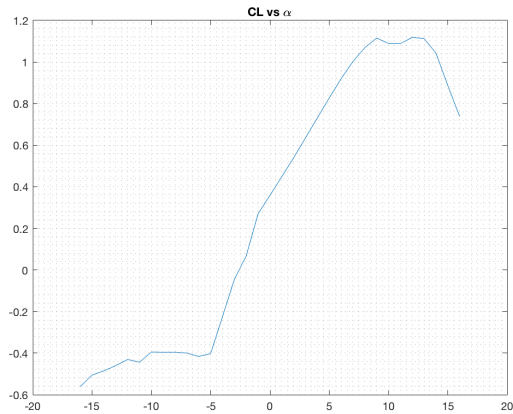


Figure 10: Forces, Moments, and Velocities in Body-Axis System

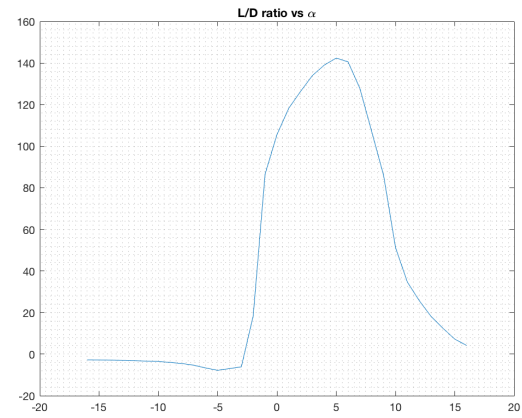
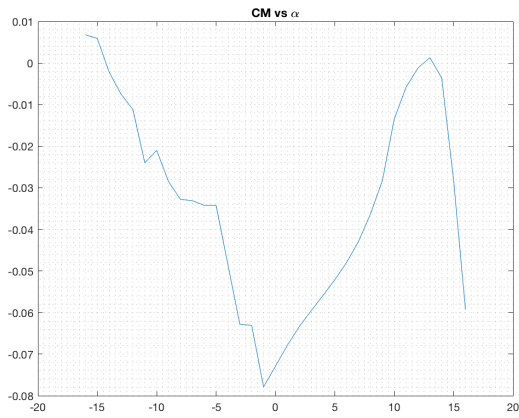
III.1.1 C_L, C_D and C_M Analysis

We measured and researched the Bixler 3 specifications and found that the airfoil shape used for the main wing is quite similar to the S3021, and the horizontal tail airfoil used is a NACA0012. For estimation purpose, we chose the Reynolds number and Mach number of our XFOIL simulations to be $Re = 120000$, $Mach = 0.03$ respectively, which corresponds to a speed of about $10m/s$. Below are the plots given by XFOIL:

Wing airfoil (S3021)

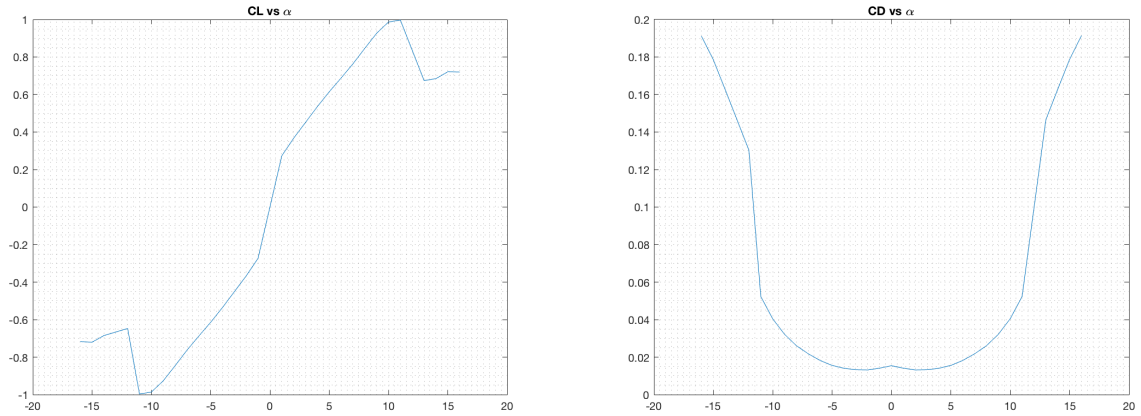


Lift and Drag Coefficients vs. Angle of Attack

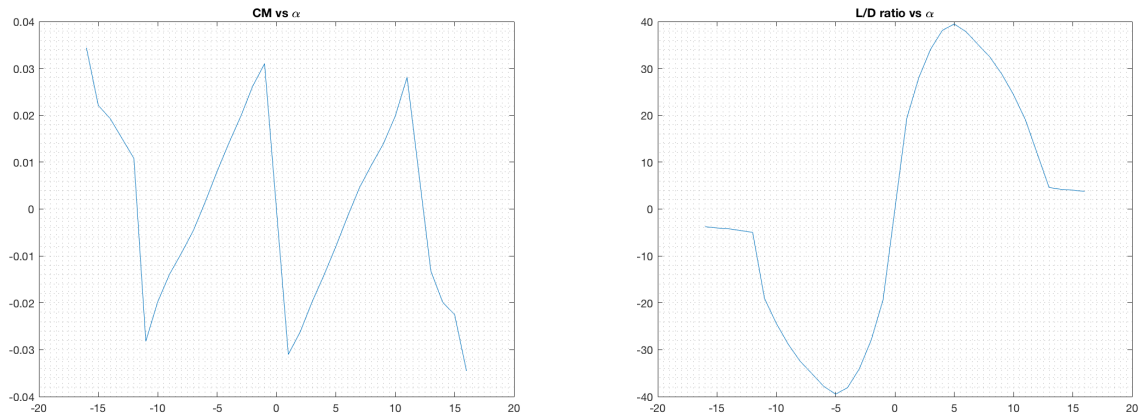


(Wing) Moment Coefficient and Lift/Drag Ratio vs. Angle of Attack

Horizontal tail airfoil (NACA0012)



(Tail) Lift and Drag Coefficients vs. Angle of Attack



(Tail) Moment Coefficient and Lift/Drag Ratio vs. Angle of Attack

III.1.2 Summary of Aircraft Parameters

Table 1: Measured Wing Geometry and Coefficient calculated from Xfoil

b	Wing span	1.55[m]
c_{root}	chord length at wing root	0.205[m]
c_{tip}	chord length at wing tip	0.09[m]
m	mass of loaded airplane	1.048[kg]
$C_{Lw,\alpha}$	Lift slope for wing	5.16[rad ⁻¹]
$C_{Lh,\alpha}$	Lift slope for tail	4.14[rad ⁻¹]
L	Length of aircraft	0.948[m]
x_{acw}	x-direction distance from nose to wing a.c.	0.32[m]
S_w	Wing Area	0.2738[m ²]
S_h	Tail Area	0.045[m ²]
$\mathcal{A}R_w$	Wing Aspect Ratio	8.77
h_h	z-direction distance between wing and tail a.c.	0.07[m]
l_h	x-direction distance between wing and tail a.c.	0.54[m]
w_f	maximum fuselage width	0.09[m]
Z_t	z-direction distance between thrust line and c.g	0.12[m]
ϵ	Wing twist	0
η_h	Tail efficiency	0.9
$\Lambda_{\frac{c}{4}}$	quarter chord sweep angle	0

$$x_{cg} \approx x_{acw} = 0.32[m] \quad (1)$$

III.1.3 Pitch Stability Analysis

The figure below shows the aircraft with no thrust:

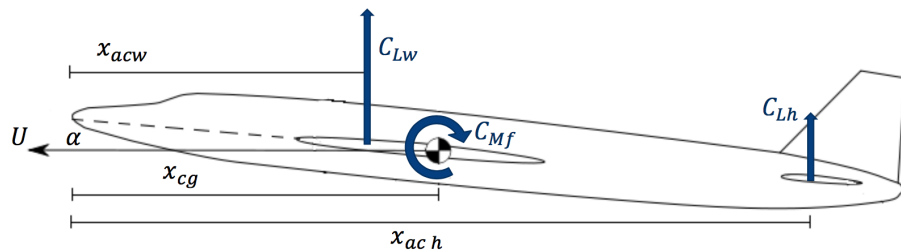


Figure 11: Aircraft with Throttle Off

A longitudinally stable aircraft must produce a sufficient pitching moment to counter any perturbation in pitch.

$$\frac{\partial C_M}{\partial \alpha} < 0 \quad (2)$$

Considering about the center of gravity:

$$\frac{\partial C_{M_{C.G.}}}{\partial \alpha} = -C_{L_\alpha w} \frac{x_{acw} - x_{cg}}{\bar{c}} + C_{M_\alpha f} - \eta_h C_{L_\alpha h} \left(1 - \frac{d\varepsilon}{d\alpha}\right) \frac{S_h}{S_w} \frac{x_{ach} - x_{cg}}{\bar{c}}, \quad (3)$$

where:

$C_{L_\alpha w}$ is the wing lift curve slope;

$C_{L_\alpha h}$ is the horizontal tail lift curve slope;

subscript ‘w’ represents wing;

subscript ‘h’ represents horizontal tail;

subscript ‘ac’ represents aerodynamic center, which is at the 1/4-chord position for low Mach, thin airfoil;

S_w and S_h are areas of wing and tail respectively;

\bar{c} is the mean aerodynamic chord defined as

$$\bar{c} = \frac{2}{S} \int_0^{\frac{b}{2}} c^2 dy \quad (4)$$

where b is the span, y is the coordinate along the wing span and c is the chord at the coordinate y .

According to NACA report 711 (<http://naca.central.cranfield.ac.uk/reports/1941/naca-report-711.pdf>), the pitching moment generated by the fuselage ($C_{M_\alpha f}$) is empirically given by:

$$C_{M_\alpha f} = K_f \frac{L_f w_f^2}{\bar{c} S_w} \quad (5)$$

where:

L_f is fuselage length;

w_f is fuselage max width.

The effect of the position of the wing along the fuselage is given by the constant K_f which is a function of the wing root 1/4 - chord position, a plot is given below where we can find approximate value of K_f :

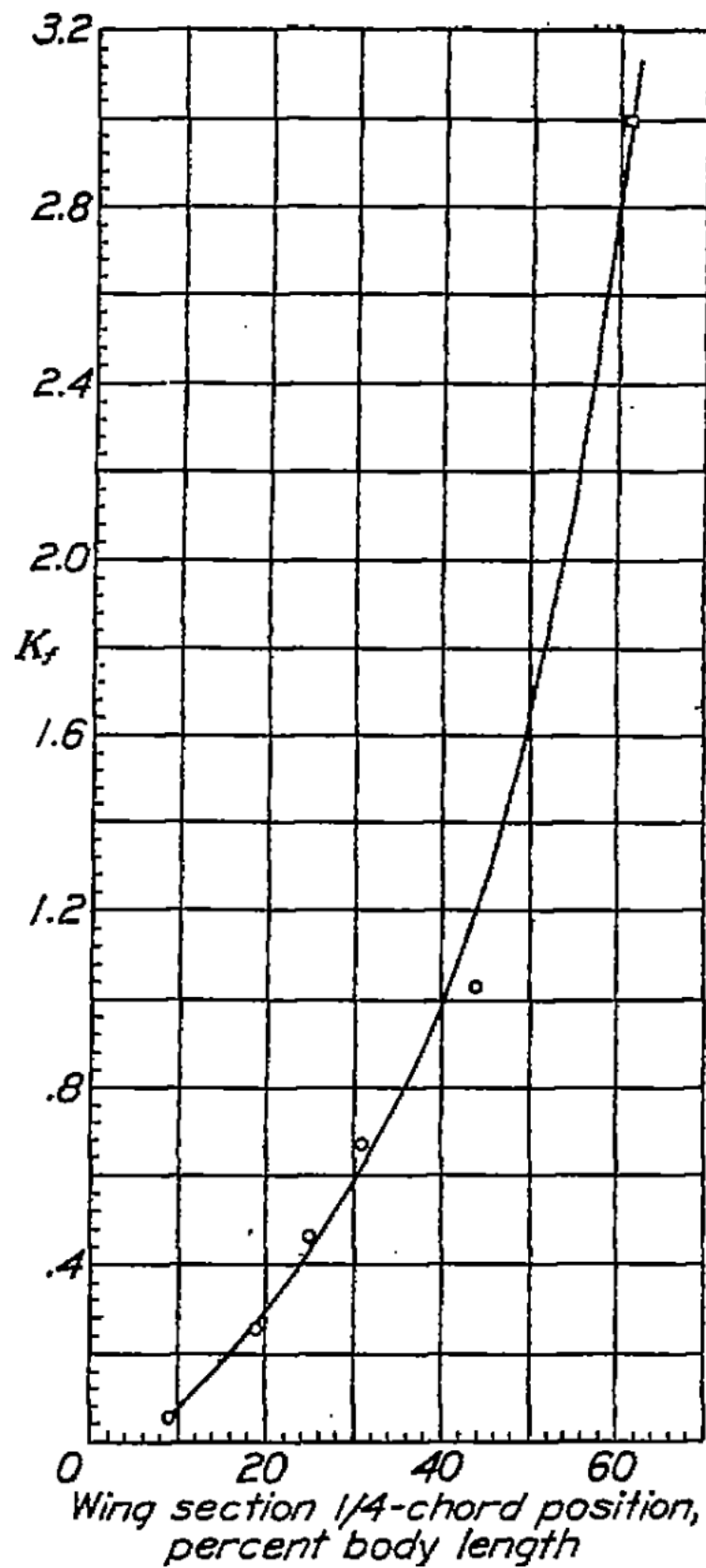


Figure 12: K_f vs. Wing 1/4-Chord Position

Based on our measurements, an approximated value is $C_{M_{\alpha}f} \approx 0.1109$.

The tail efficiency factor η_h accounts for difference between the dynamic pressure at the tail and that in the free stream, typical value is:

$$\eta_h \begin{cases} \approx 0.9 & \text{for low tails} \\ \approx 1.0 & \text{for T-tails} \\ > 1.0 & \text{for blown tailplane} \end{cases} \quad (6)$$

In our case, Bixler has low tails, so $\eta_h \approx 0.9$.

The variation of downwash angle with wing angle of attack is given empirically by

$$\frac{d\varepsilon}{d\alpha} = 4.44 \left(K_A K_\lambda K_h \sqrt{\cos \Lambda_{c/4}} \right)^{1.19} \frac{C_{L_\alpha w} \Big|_M}{C_{L_\alpha w} \Big|_{M=0}}, \quad (7)$$

where $\Lambda_{c/4}$ is the $1/4$ - chord sweep angle, and

$$K_A = \frac{1}{\mathcal{A}} - \frac{1}{1 + \mathcal{A}^{1.7}} \quad (8)$$

$$K_\lambda = \frac{10 - 3\lambda}{7} \quad (9)$$

$$K_h = \frac{1 - |h_h/b|}{\sqrt[3]{2l_h/b}} \quad (10)$$

\mathcal{A} is the aspect ratio, and λ is the taper ratio. They are given by:

$$\mathcal{A} = \frac{b^2}{S} = \frac{b}{\bar{c}}, \quad \lambda = \frac{c_{\text{tip}}}{c_{\text{root}}} \quad (11)$$

The figure below illustrates some of the variable used here:

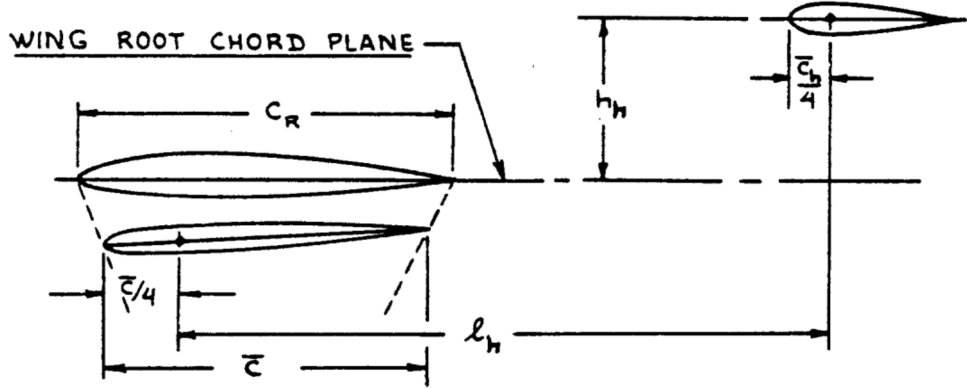


Figure 13: Illustration of Parameters

By substituting the measured parameters and theoretical values from XFOIL into eqn.(3), we found that

$$\frac{\partial C_{M_{C.G.}}}{\partial \alpha} = -1.0807 < 0, \quad (12)$$

which tells us that Bixler 3 should be statically longitudinally stable under conditions around $Re \approx 120000$, $Mach \approx 0.03$ (or flight speed of about $10 - 15m/s$).

III.1.4 Neutral Point

The C.G. position that would not result in a pitching moment with changing angle of attack is the neutral point (aircraft's aerodynamic center). It is given by setting $\frac{\partial C_{M_{C.G.}}}{\partial \alpha} = 0$ in Eqn.(3) and find the corresponding x_{cg} :

$$\frac{x_{np}}{c} = \frac{C_{L_{\alpha}w} \frac{x_{acw}}{c} - C_{M_{\alpha}f} + \eta_h C_{L_{\alpha}h} \left(1 - \frac{d\varepsilon}{d\alpha}\right) \frac{S_h}{S_w} \frac{x_{ach}}{c}}{C_{L_{\alpha}w} + \eta_h C_{L_{\alpha}h} \left(1 - \frac{d\varepsilon}{d\alpha}\right) \frac{S_h}{S_w}} \quad (13)$$

The aircraft's aerodynamic center (x_{np}) must be aft of the aft most C.G. position to ensure static stability.

From the parameters, the neutral point is found to be $x_{np} = 0.3545[m]$, which is slightly aft of the C.G. ($x_{cg} = 0.32[m]$) as it is required.

III.1.5 Trim Analysis

In a trimmed flight, we know that:

- Sum of pitching moments about c.g. is zero.
- Sum of lift forces equal weight

The figure below shows the aircraft in trimmed flight:

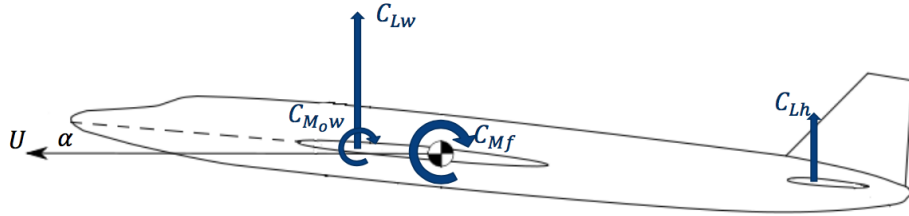


Figure 14: Aircraft in Trimmed Flight

The pitching moment about c.g. and total lift are given by:

$$C_{M_{C.G.}} = -C_{Lw} \frac{x_{acw} - x_{cg}}{\bar{c}} + C_{M_{0w}} + C_{M_{\alpha f}} \alpha - \eta_h C_{Lh} \frac{S_h}{S_w} \frac{x_{ach} - x_{cg}}{\bar{c}} + \frac{Z_t T}{q S_w \bar{c}}, \quad (14)$$

$$C_L = C_{Lw} + \eta_h \frac{S_h}{S_w} C_{Lh}. \quad (15)$$

The **wing's** zero lift pitching moment is empirically given by:

$$C_{M_{0w}} = \left[C_{m_0 air} \left(\frac{\mathcal{R} \cos^2 \Lambda_{c/4}}{\mathcal{R} + 2 \cos \Lambda_{c/4}} \right) - 0.01 \epsilon \right] \times 1.3, \quad (16)$$

where:

$C_{m_0 air}$ is **airfoil** zero lift pitching moment, which can be found by using XFOIL;

ϵ is wing twist in degrees, in our Bixler, there is no(or negligible) wing twist.

For steady level flight:

$$T = q S_w C_D, \quad q = \frac{1}{2} \rho U^2, \quad (17)$$

and Z_t is the distance between vertical c.g. and thrust line (positive if thrust line under c.g.).

III.2 Experimental results

III.2.1 $\max C_L$, $\max L/D$, stall speed and drag parameter analysis

To calculate the maximum lift coefficient of the Bixler, we first solved for the lift and drag of the aircraft. The Pixhawk took an enormous amount of data from our flight test so to simplify the amount of data processing, only data with no throttle input and a roll angle between $+/-3$ degrees was used. Then a free-body diagram was drawn with both the wind and body axes present as well as the lift, drag, and weight forces.

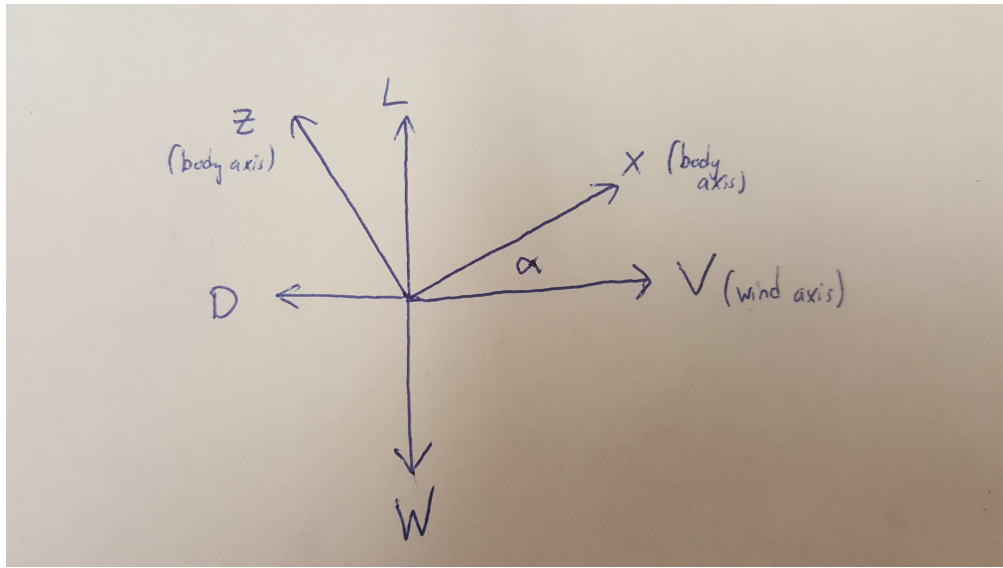


Figure 15: Free Body Diagram of Bixler with No Throttle

The summation of forces was then taken in both the x and z directions.

$$ma_x = L \sin \alpha - W \sin \alpha - D \cos \alpha \quad (18)$$

$$ma_z = L \cos \alpha + D \sin \alpha - W \cos \alpha \quad (19)$$

This gives two equations for the two unknowns L and D. The angle of attack α is the z velocity component divided by the u velocity component and a_x and a_z are the body axis accelerations in the x and z directions. Because the accelerometer is raw, the gravity component was subtracted from each body axis acceleration based on the pitch angle.

$$a_{xnew} = a_x + g * \sin \alpha \quad (20)$$

$$a_{znew} = a_z - g * \cos \alpha \quad (21)$$

Once these body axis accelerations were corrected, a simple matrix inversion can solve for the lift and drag for each point given mass, weight, pitch angle, and acceleration.

These lift and drag calculations can immediately be used to solve for L/D .

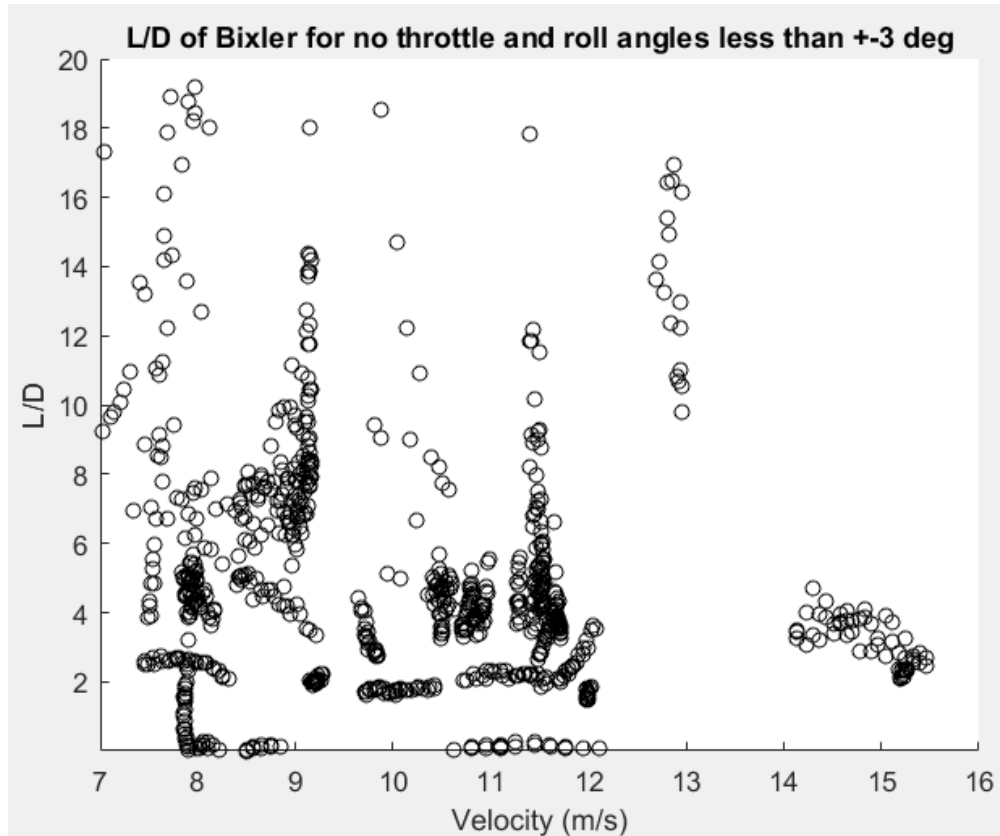


Figure 16: L/D vs. Vel for Bixler 3

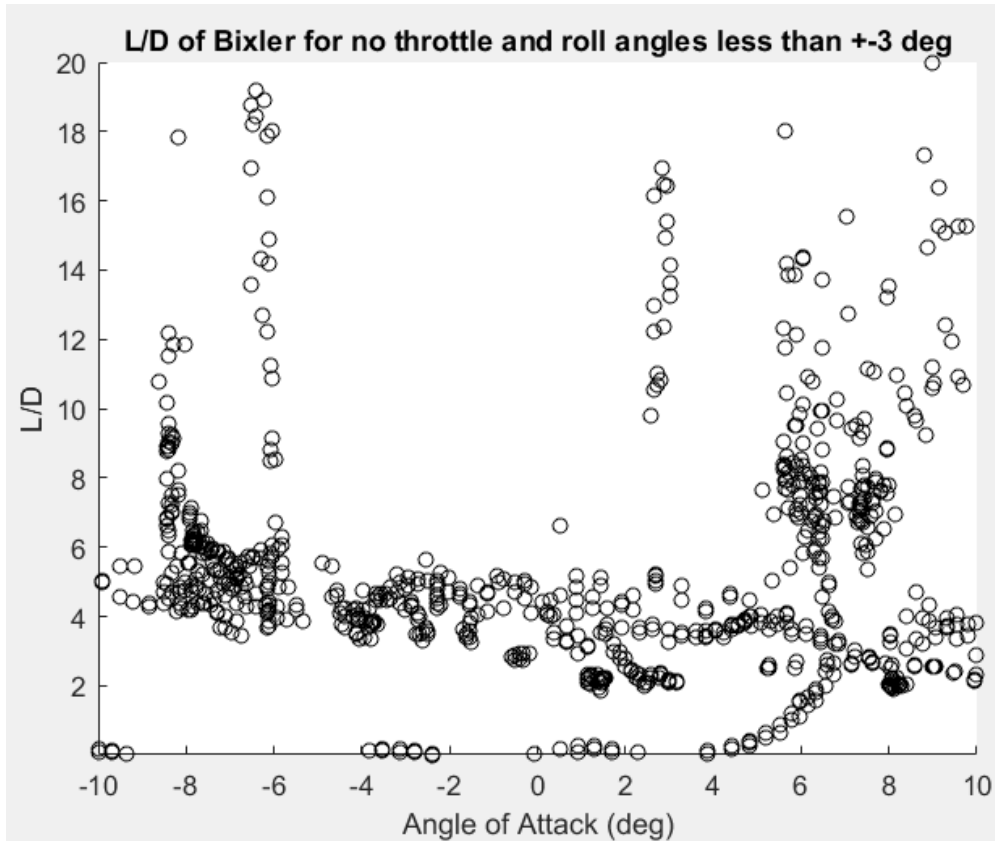


Figure 17: L/D vs. Angle of Attack for Bixler 3

It is difficult to determine a trend from the L/D data. Theoretically, for a constant lift, L/D should be parabolic with the peak at a given velocity. The plot against velocity somewhat resembles a parabola, but has many outlying data points and also multiple lift-to-drag ratios for a given velocity. This could be due to several factors. For one, the flight test of the Bixler contained very little steady flight data. Most of the time the plane was rolling or pitching up and down. The wind velocities were between 10 and 15 MPH that morning which was causing a lot of problems trying to keep the plane stable. Also, because the wind velocity wasn't directly measured from the Pixhawk but rather estimated from weather reports, the true velocity in the u direction wasn't what the data indicated. An effort was made to try to account for the wind while data processing, but a constant wind speed had to be used which won't be entirely correct due to gusts and unsteadiness as well as changes in altitude. Overall, the L/D data isn't great, but the magnitude appears to be reasonable. The expected maximum lift-to-drag ratio given in class was about 12 and this is nearly the peak L/D in our data. Our data indicates a maximum L/D to be approximately between 12 and 18.

The lift coefficient was trivial to find after already calculating the lift and velocity for each data point. The equation for lift coefficient is given as:

$$C_L = \frac{L}{\frac{1}{2}\rho V^2 S_w} \quad (22)$$

Using the measured wing area and an air density for just above sea level, the lift coefficient was calculated for each data point. Lift coefficient vs alpha is shown in the figure below.

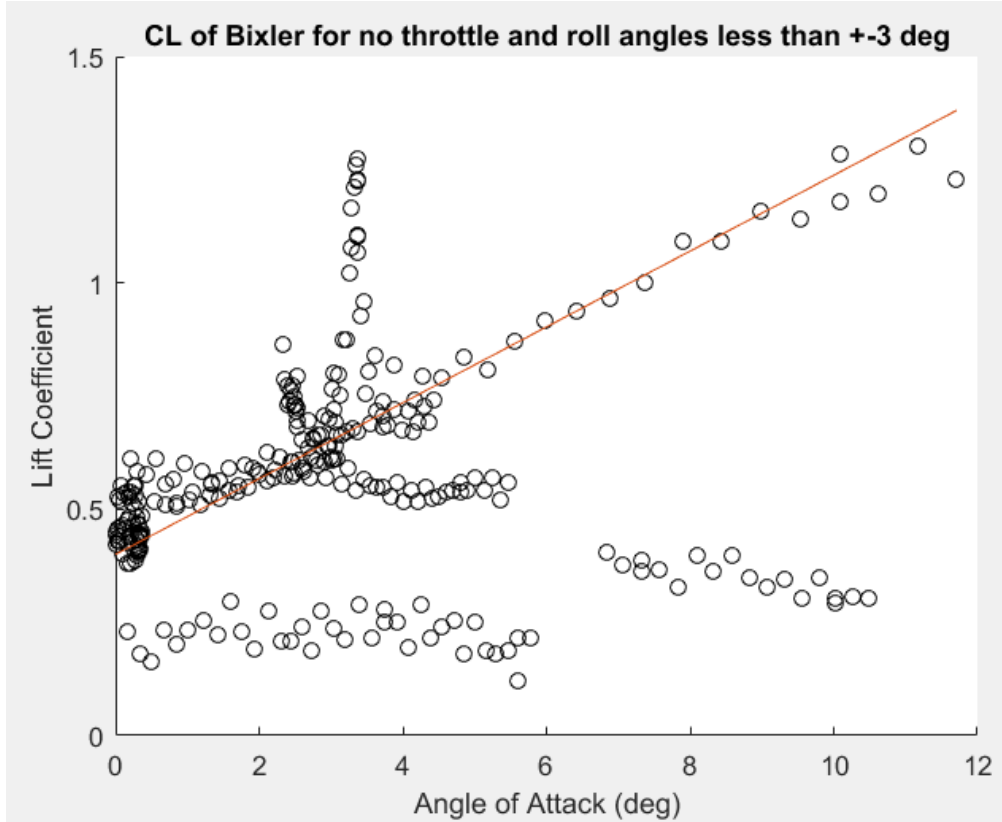


Figure 18: C_L vs. α for Bixler 3

This data turned out much nicer than the L/D. As expected, there is a linear trend between the lift coefficient and angle of attack. The lift coefficient at zero angle of attack is 0.4 which matches well with the theoretical value calculated in XFOIL. The slope of the curve is 4.8. This is slightly lower than expected, but still reasonable. In a 2-dimensional case, the lift curve slope would be 2π however 3-dimensional effects will lower this value so 4.8 makes sense. From the data, the maximum lift coefficient appears to be about 1.3. However there are only a couple data points to justify this claim and they could be outliers. The bulk of the data supports a maximum lift coefficient of at least 0.8, with the possibility that it could reach up to 1.3.

The maximum lift coefficient can also be used to approximate the stall speed of the aircraft. We will use a maximum lift coefficient of 1.0 to solve for the stall speed for steady, level flight. Taking lift to be weight in this case and plugging the appropriate values into the C_L equation given above, the stall velocity can be calculated to be approximately 7.2 m/s.

The zero-lift drag coefficient can also be computed from the data gathered. After some variable manipulation, the zero-lift drag coefficient can be written as:

$$C_{D_0} = \frac{DC_L}{L} - \frac{C_L^2}{\pi \cdot e \cdot A_w} \quad \text{with} \quad C_d = C_{D_0} + C_{D_i} \quad (23)$$

The e parameter represents the Oswald coefficient and is usually of about 0.8 to 0.9. Theoretically the computed parameter is equal at any time during flight; the computed average C_{D_0} is 0.0913, taking into account straight-line - roll less than 5 degrees - level-flight without thrust. From here the maximum Lift to drag ratio can be formally computed using the following relation

$$\max \left(\frac{L}{D} \right) = 0.5 \cdot \sqrt{\frac{\pi b^2}{S \cdot C_{D_0}}} \quad (24)$$

Experimentally we were able to compute an maximum lift to drag ratio of 16.398 [-], which matches fine the plotted relation displayed in Figure 17.

III.2.2 Pitch Stability Analysis

The moment about x,y,z body axis of the plane \vec{M} is essentially the inertial derivative of angular momentum \vec{H} of the plane, which is the moment of inertia matrix \mathbf{I} multiplied by the angular velocity $\vec{\omega}$. For steady level flight, the moment \vec{M} can be expressed in Eq.25, where the higher order term of the angular velocity perturbation can be negligible.

$$\vec{M} = {}^I \vec{H} = {}^I ([\mathbf{I}] \vec{\omega}) = I \dot{\vec{\omega}} + H.O.T. \quad (25)$$

The time derivative of \mathbf{I} goes to zero since body axis are body fixed frame. Therefore, the pitching moment $M_y = I_{yy}\dot{q}$. To check for the pitch stability for the aircraft from the experimental data, we need to find the change of pitch moment with respect to the change in angle of attack ($\frac{\partial M_y}{\partial \alpha}$). Since the pitch moment M is proportional to the time derivative of pitch rate \dot{q} (I_{yy} is a constant), $\frac{\partial \dot{q}}{\partial \alpha}$ can represent the tendency of M_y when varying α . \dot{q} was extracted from the data by numerically differentiating the pitch rate data. α was calculated as $\frac{w}{u}$. Data from straight flight segment were extracted to plot \dot{q} against change in α as

shown in Fig.19.

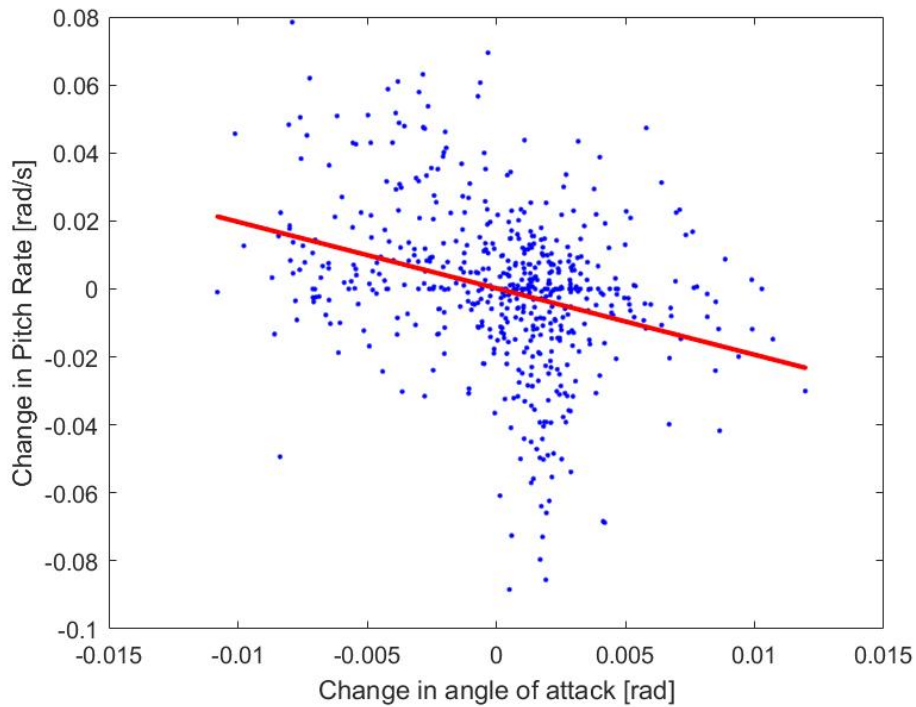
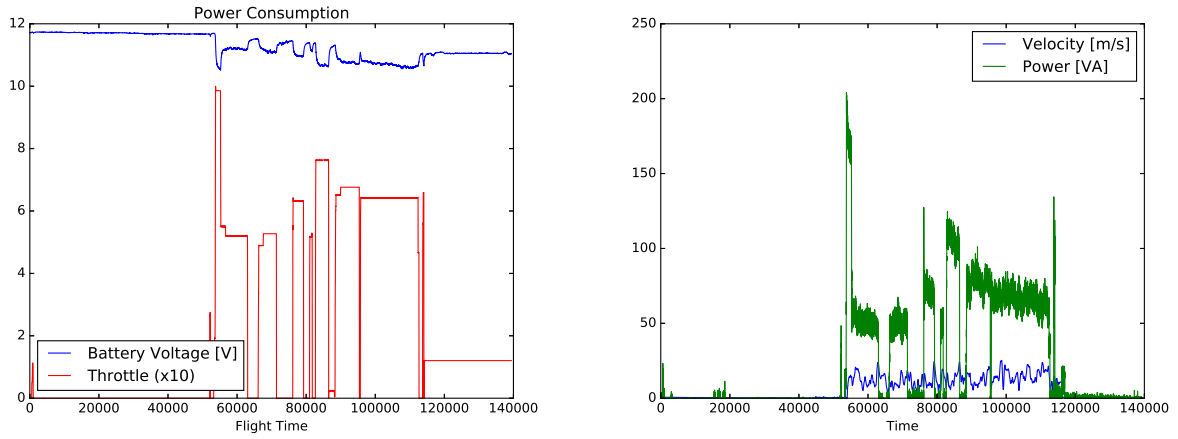


Figure 19: \dot{q} vs. change in α

The red line shows the linear fit for the scattered data, which has a negative slope. The proportionality between \dot{q} and M_y yields that $\frac{\partial M_y}{\partial \alpha} < 0$. This confirms that this aircraft is pitch-stable.

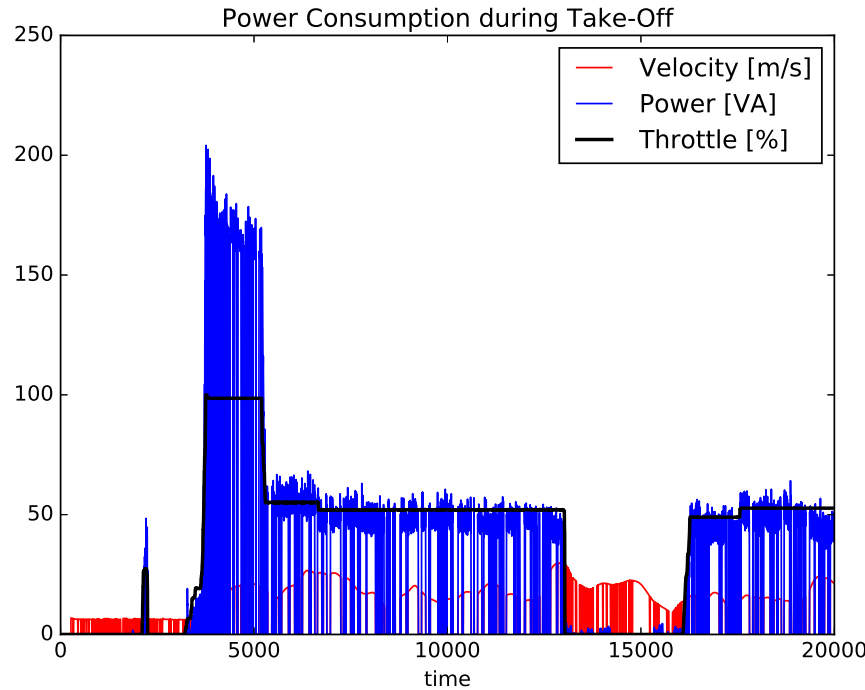
III.2.3 Power Consumption

Ideally the power consumption would be measured and computed in steady level flight for different velocities. The following plots are based on the same set of data as all our previous data analysis.



In these first two graphics show the evident relation between the decreasing battery voltage and the throttle activity over the flight time. The first peak in the throttle curve represents the take-off. And as we can see, actual gliding-time, i.e. flight time with no thrust involved , is very limited.

As one might notice, defining a clear relation between velocity and power consumption is quite difficult due to other factors involved and acting on the velocity term, like irregular flight paths or wind to name two examples.



In this third graphical representation regarding the power consumption of the Bixler, three variables are taken into account to highlight the their interrelation.

When computing the velocity an estimation of the wind conditions during test flight has been taken into account. The throttle activity is given in % and one clearly sees an relation between throttle and power . As expected with no active throttle the power output in the flight system is zero., which is due the linear relation of : $P = V * I$. The throttle is our main energy consumer, which is expected since the required energy of the servo-motors is fairly low.

Most interestingly, during take-off the initial *pull up*, engaging 100% of the throttle's capacity requires more power than expected. Why using the take-off as a reference for this analysis? It is , compared to other segments of our flight path, a straight flight along the body's x-axis. Further the take-off maneuver is directed against the wind, which makes taking its effect on our velocity quite easy to implement.

III.2.4 Control Effectiveness Analysis

To test the control effectiveness, the corresponding response is plotted against the control input. RC command input is a value between -1 and 1, which can be linearly mapped to the deflection angle on the control surfaces, which will have an effect on the aircraft rotation. Pitch rate is plotted with RC elevator control input, as shown on the left of Fig.20. This shows a positive linear trend, which shows that longitudinal control is effective. With maximum elevator deflection, the pitch rate can reach as high as 2.8[rad/s]. Both the response and input are plotted against time around a trimmed point in order to see the promptness of the response after receiving the command, as shown on the right of Fig.20.

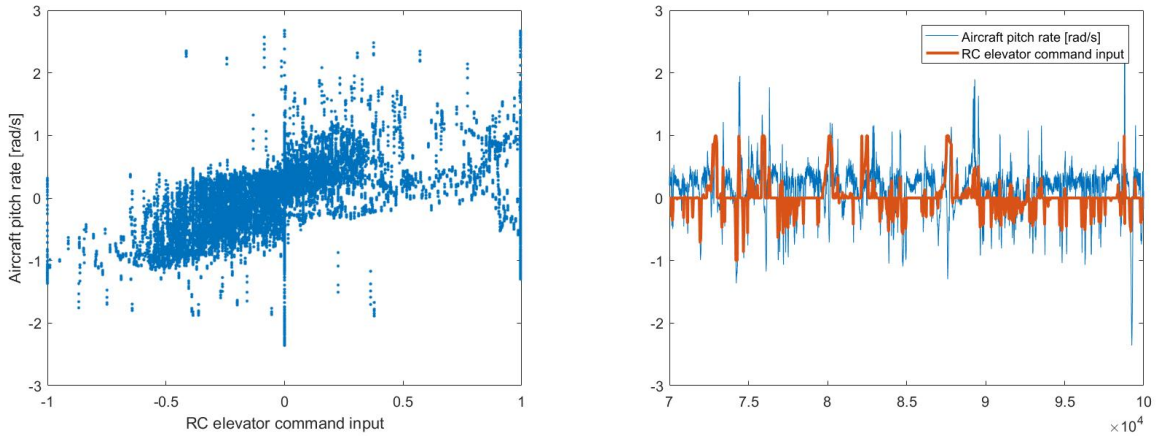


Figure 20: Aircraft pitch rate vs. RC elevator command input

It can be seen that the response has a very small delay, which shows that the longitudinal control is almost immediately effective.

Similarly, for lateral control effectiveness, roll rate was plotted against RC aileron command input, as shown on the left of Fig.21. It can also be seen from the positive linear trend that the response follows the command effectively. The right of Fig.21 plotted both the roll rate and RC aileron input against time around a trimmed point, and it shows that the lateral control has a longer delay in response than the longitudinal control.

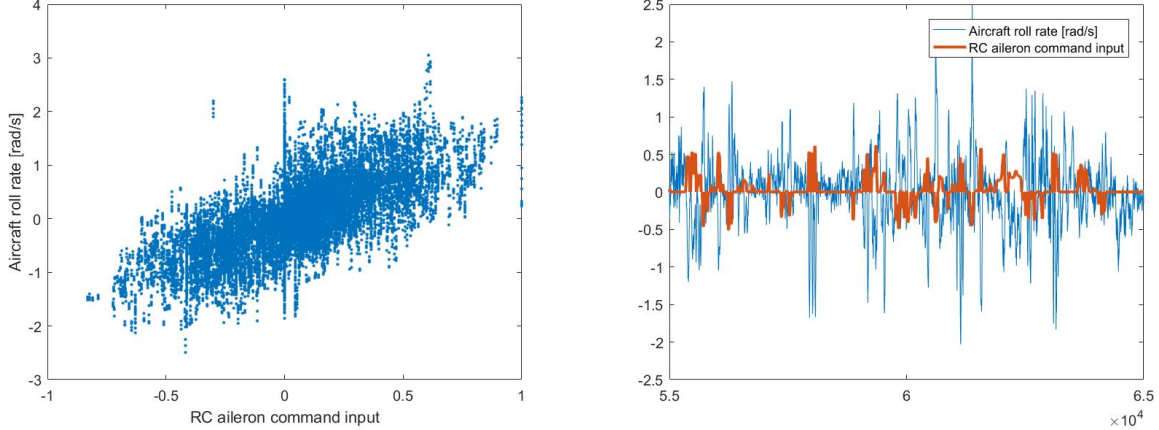


Figure 21: Aircraft roll rate vs. RC aileron command input

IV Preliminary Mission Strategy

While the specific details of the mission are not fully specified yet, we know that broadly, the goals of the mission are to visit points of interest with different scientific values, while minimizing energy consumed and maximizing the scientific value. This task can be thought of in terms of three main hierarchies of control problems:

1. **Decision Making:** Which point of interest should the plane fly toward?
2. **Path Planning:** Given a desired goal point, what flight path should the plane take to visit that point with minimal energy consumption?
3. **Servo Control:** Given a desired flight path, how should the control surfaces be actuated to achieve it?

In the following subsections, we discuss strategies to solve each level of control problem.

IV.1 Decision Making (Trajectory Planning)

The problem of choosing goal positions for the aircraft to fly is related to the traveling salesman problem, an NP-Complete problem which can quickly become intractable as the

number of goal positions to choose from increases. The fact that we must also consider energy consumption and goal position value in computing the order in which to visit the goal positions makes solving this problem exactly quite difficult. Instead, we plan to use heuristics and approximate solution methods such as simulated annealing or evolutionary methods to quickly come up with an ordered selection of the waypoints that performs well on the combined objective of minimum energy and maximum value.

In order for the waypoints selected to be realistic, we must plan these paths under the constraint of a maximum energy consumed. Thus, the trajectory planner will require a method $E \approx f(p_1, p_2, \Delta t)$ which approximates the energy required to fly from state p_1 to state p_2 in time Δt .

IV.2 Path Planning

Given an immediate next goal position, the problem of finding a control input that optimizes energy consumed can be viewed as an optimal control problem. We can define a cost functional J corresponding to the energy of a trajectory as follows:

$$J = \int_0^{t_f} g(\mathbf{x}(t), \mathbf{u}(t)) dt$$

where $\mathbf{x}(0), \mathbf{x}(t_f), t_f$ are fixed and $g(\mathbf{x}(t_f), \mathbf{u}(t_f))$ is the power required at state $\mathbf{x}(t)$ with control input $\mathbf{u}(t)$. Our goal is to find $\mathbf{u}(t)$ such that together with the resulting state trajectory $\mathbf{x}(t)$, the cost functional J is minimized. To keep the optimization problem tractable, we plan to consider our control input $\mathbf{u}(t)$ as the aircraft velocity and turning rate, assuming that a lower level of control will be able to maintain the commanded values. From flight testing, we will be able to characterize our plane to compute the bounds on both commanded velocity and turning rate.

We plan to solve for open loop solutions to this problem, and recompute optimal trajectories at some regular interval to account for noise and disturbances.

IV.3 Servo Control

The lowest level control is that of choosing throttle and control surface levels in order to maintain the commanded velocity and turning rate given by the path planning solution. We plan to apply techniques from nonlinear control to design controllers that provide fast and stable dynamics on velocity and turn rate.

It is important to note that this hierarchy of control will only work if each level operates with good models of the levels under it - i.e. the system will not work if the path planning

is done under unrealistic assumptions of turning rate or velocity controllability.

IV.4 Additional Comments

The above strategy should handle missions that only require flyovers of the points of interest. If instead the mission requires that the plane should loiter at a given location, we may need multiple control modes, one to fly along a path and another to maintain position at a certain location.

V Goals and Plan of Action

After this homework assignment is completed, the plan is to get ready for the design of our Mars aircraft. While the mission and required aircraft parameters aren't completely known yet, our group will begin dividing up tasks to prepare for the design. Some of our group will take the Bixler aircraft characteristics and use them to construct a plant and design controllers for the Bixler to fly autonomously. This will be great practice for when we have to do the same with our Mars aircraft. Others of us will focus on the physical design of the new plane, and the wing most notably. In a first step, we will be using XFLR5 to design the wing profiles and entire plane configuration to then be looking into the various ways of manufacturing the drafted prototype design. Most likely, the chosen materials will be including low-density foam, and some type of polymer to use for 3D printing.